ACS OMEGA

http://pubs.acs.org/journal/acsodf

Article

Effects of Plasticizers and Clays on the Physical, Chemical, Mechanical, Thermal, and Morphological Properties of Potato Starch-Based Nanocomposite Films

Hasanul Banna Muhammad Zukaul Islam, Md. Abu Bin Hasan Susan, and Abu Bin Imran*

Cite This: *ACS Omega* 2020, 5, 17543−17552

Read Online

ACCESS | Metrics & More | Article Recommendations | Supporting Information

ABSTRACT: Biodegradable polymeric films have great potential as alternatives to synthetic polymeric films to reduce environmental pollution. Plasticizing agents and nanofillers can improve the mechanical properties of polymer-based composites, resulting in materials with better flexibility and extensibility. Starch, a natural polymer, can be produced at low cost and on a large scale from abundant and inexpensive agricultural resources like potatoes. The aim of the present work was to fabricate mechanically strong and thermally stable potato starch films reinforced with different types of plasticizers and nanoclays at different concentrations. Different types of plasticizers such as water, glycerin, ethylene glycol, sorbitol, and formamide and three types of clays such as montmorillonite, hectorite, and kaolinite at various concentrations were used to prepare potato starch-based nanocomposite films. The films were prepared using a very simple solution casting process. The mechanical properties and thermal stabilities of nanocomposite films significantly improved using montmorillonite, hectorite, and kaolinite clays. The water uptake percentage of the fabricated films decreased with addition of plasticizers and further decreased with addition of different types of clays. The structural and morphological changes of the fabricated films in the presence of plasticizers and nanoclays were correlated in detail with their mechanical properties, crystallinity, biodegradability, thermal stability, and water absorption capacities.

INTRODUCTION

Polymeric films based on natural/biopolymers are in high demand due to their environmentally friendly nature in contrast to their synthetic or non-biodegradable counterparts, which are associated with several environmental issues like soil degradation, loss of soil fertility, blocking up of drainage and sewerage systems, causing water logging, and the spread of harmful microbes and bacteria. Polymers derived from renewable sources include naturally existing proteins, cellulose, starches, and other polysaccharides, and those synthesized chemically from naturally derived monomers are known as natural/biopolymers. Among all biopolymers, natural starch is one of the leading candidates as it is an abundant and low-cost natural resource for biodegradable polymeric materials. It is a semicrystalline polymer stored in granules as a reserve in most plants and is composed of repeating 1,4-α-D-glucopyranosyl units of amylose and amylopectin chains.[1] Amylose is primarily a linear molecule with α-1-4-linked glucosyl units. Amylopectin is a highly branched molecule, with (1 → 4)-linked α-D-glucosyl units in chains joined by (1 → 6) linkages. Generally, amylose has a high tendency to retrograde and produce tough gels and strong films, whereas amylopectin, in an aqueous dispersion, is more stable and produces soft gels and weak films.[2]

With necessary modifications or processing, starch can be used as an ideal biopolymer that comes from nature and readily returns to nature. Unfortunately, most of the reported starch-based materials exhibit poor tensile strength, yield strength, stiffness and elongation at break, and water repulsion capacity.[3,4] It can be processed as a thermoplastic material only in the presence of plasticizers and under the action of heat and shear. Accordingly, many low-molecular-weight materials such as water, ethylenebisformamide, urea, glycerin, ethylene glycol, formamide, sorbitol, and xylitol have been investigated for their plasticizing abilities.[5−8] Formulations of thermoplastic starch composite films with poly(vinyl alcohol) (PVA), ethylene−acrylic acid (EAA), polyethylene (PE), polyesters including polycaprolactone and poly(hydroxybutyrate-valerate) (PHBV), and polyamides have been reported. These fabricated composite films generally showed an increase in elongation while decreasing tensile strength and embrittled with age.[9−11]

Polymer nanocomposite materials are often easy to process and provide property enhancements extending orders of magnitude beyond those realized with traditional polymer composites. Carbon nanotubes (CNTs),[12−14] layered silicate

Received: May 1, 2020
Accepted: June 19, 2020
Published: July 7, 2020

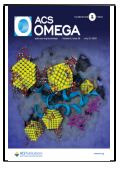

https://dx.doi.org/10.1021/acsomega.0c02012
ACS Omega 2020, 5, 17543−17552

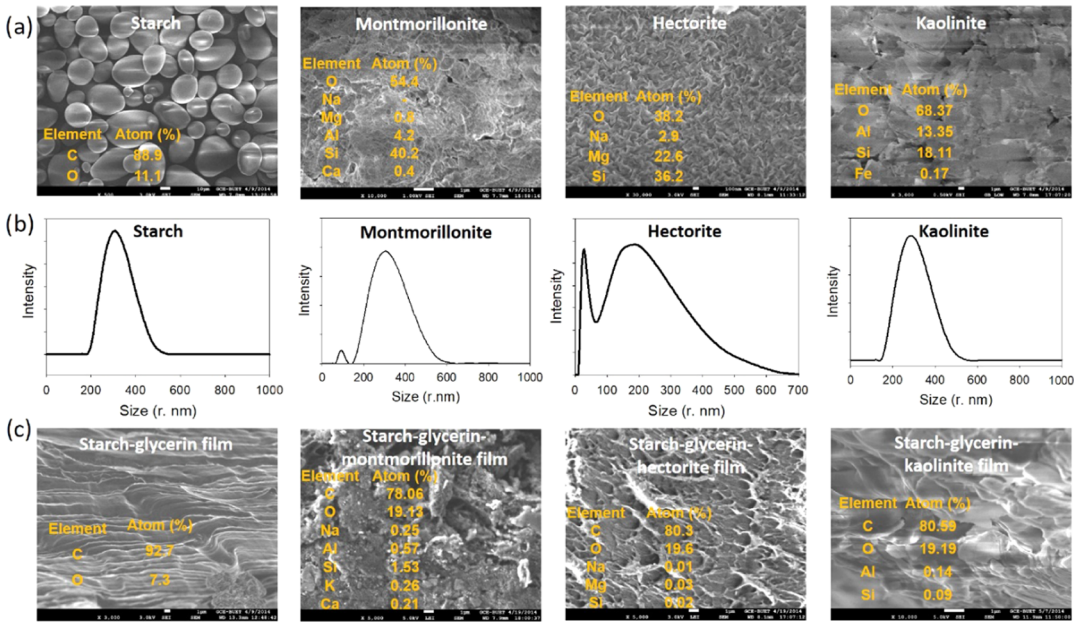

Figure 1. (a) SEM images of extracted potato starch, montmorillonite nanoclay, hectorite nanoclay, and kaolinite nanoclay. (b) DLS of extracted potato starch, montmorillonite nanoclay, hectorite nanoclay, and kaolinite nanoclay. (c) SEM images of starch−glycerin film, starch−glycerin−montmorillonite nanocomposite film, starch−glycerin−hectorite nanocomposite film, and starch−glycerin−kaolinite nanocomposite film.

clay nanoparticles,[15−17] cellulose nanocrystals,[18] graphite nanoflakes,[19−21] etc. are the examples of commonly used reinforcements. The use of clay nanoparticles as precursors to nanocomposite formation has been investigated in various polymer systems including starch,[22−24] nylon 6,[25,26] epoxys,[27] polyamides,[28,29] polystyrenes,[30] polyurethanes,[31] polypropylene,[32−36] polyethylene,[37,38] and so on. Incorporation of nanoclays into starch matrixes may be valued in terms of their superior mechanical and thermal performance for their application as highly competent biodegradable materials. These clays are environmentally friendly, naturally abundant, and economical. Clays are classified into three types according to the type and the relative content of the unit crystal lamellae: 1:1 type (unit lamellar crystal is composed of one crystal sheet of silica tetrahedron combined with one-crystal lamellae of alumina octahedron), 2:1 type (unit lamellar crystal is composed of two crystal sheets of silica tetrahedron combined with one crystal sheet of alumina octahedron between them), and 2:2 type (unit lamellar crystal is composed of four crystal sheets, in which crystal sheets of silica tetrahedron and alumina or magnesium octahedron are alternately arranged).The most commonly used nanoclays for the preparation of polymer nanocomposites belong to the family of 2:1 phyllosilicates and, in particular, smectite clays as they have a unit layer structure in nanodimensions and layers are expandable and easily exfoliated during formation of the nanocomposite. Although there are some reports on starch−clay-based nanocomposite films[39−44] in the literature, systematic approaches of using different types of clays and plasticizers to obtain superior starch−clay nanocomposite films are scarce. Even the highly abundant potato starch-based nanocomposite films are not widely investigated. While the reinforcement of nanocomposite films is the key area of interest, a number of other properties including thermal stability, low water absorption capacity, and low crystallinity are required to obtain biodegradable films as alternatives to synthetic plastics.[45−52]

In this work, an attempt has been made to fabricate starch−clay nanocomposite films by incorporating different types of clay nanoparticles and plasticizers into the potato starch polymer network. A facile and simple solution casting method has been employed for the synthesis of mechanically strong starch-based nanocomposite films, which are comparable to synthetic polymers, for example, polyethylene, polypropylene, polystyrene, poly(ethylene terephthalate), and so on. The physicochemical characteristics including superior mechanical strength, thermal stability, water expulsion capacity, crystallinity, and biodegradability of the synthesized nanocomposite films have been correlated with their morphological and structural changes.

RESULTS AND DISCUSSION

The starch granules extracted from potato are round or oval in shape with smooth surfaces and have a wide distribution of sizes ranging from several hundred nanometers to a few micrometers (Figure 1). Only carbon and oxygen peaks appear in the energy-dispersive X-ray spectrometer (EDS) spectrum where the elemental percentages of carbon and oxygen are found to be 88.90 and 11.10%, respectively. The hydrodynamic radius of extracted potato starch is found to be 302 nm from the dynamic light scattering (DLS) analysis. Strong inter- and intramolecular hydrogen bonds exist in starch molecules. When starch molecules come in contact with water, a strong interaction between the starch and water molecules at the interfaces occurs, which acts like a surfactant to keep starch particles apart and prevent agglomeration and precipitation. The average ζ-potential value for starch granules is −18 mV, which indicates the relatively poor stability of starch particles in water. Nanoclays are very thin and of irregular shapes and their size ranges widely as confirmed from scanning electron microscopy (SEM), DLS, and X-ray diffraction (XRD) analysis. We used two 2:1 type nanoclays, one is montmorillonite and the other one is hectorite, and a 1:1 type kaolinite nanoclay. Montmorillonite is a derivative of pyrophyllite with a

https://dx.doi.org/10.1021/acsomega.0c02012
ACS Omega 2020, 5, 17543−17552

2:1 layer structure consisting of two fused silica tetrahedral sheets sandwiching an edge-shared octahedral sheet of alumina. All positions at the top and base of lattice layers of montmorillonite are completely occupied by oxygen atoms, and these layers are held together by a relatively weak intermolecular force. In a polar solvent, such as water, this intermolecular force is broken and the basal distance of the silicate layers increases by solvation of the cation, leading to exfoliation of silicate layers into individual sheets. The chemical formula of montmorillonite is $(Al_{3.34}Mg_{0.66})$-$(Si_{7.0}Al_{1.0})O_{20}(OH)_4$. The SEM image of montmorillonite depicts large aggregation. It contains oxygen, magnesium, aluminum, silicon, and calcium with elemental percentage of 54.41, 0.81, 4.21, 40.23, and 0.33%, respectively, which coincides with its chemical composition. The average hydrodynamic radius of montmorillonite is 300 nm (Figure 1). The ζ-potential value of montmorillonite is −20.9 mV, indicating its poor stability in water. Hectorite, a 2:1 type smectic clay, is a soft, white clay mineral with a chemical formula of $Na_{0.3}(Mg, Li)_3Si_4O_{10}(OH)_2$. The hectorite nanoclay granules usually exist as a sheet in a suitable dispersion medium, but in the powdered form, granules appear as spherical particles ranging from several hundred nanometers to a few micrometers due to the strong aggregation factor. The elemental percentages of oxygen, sodium, magnesium, and silicon in hectorite clay are 38.17, 2.91, 22.64, and 36.27%, respectively, consistent with its chemical composition. The average hydrodynamic radius of hectorite clay in water is found to be 155 nm (Figure 1). Its ζ-potential value is −32.3 mV indicating the moderate stability of hectorite clay in water. Kaolinite, a 1:1 type of layered mineral, is composed of one tetrahedral sheet and one octahedral sheet. The basal oxygen atoms of the tetrahedral sheet form a hexagonal pattern and the apical or top oxygen atoms of all tetrahedra are perpendicular to the sheet. The tetrahedral and octahedral sheets of kaolinite are connected with shared oxygen atoms. The chemical formula of kaolinite is $Al_4[Si_4O_{10}](OH)_8$. The elemental percentages of oxygen, aluminum, silicon, and iron in kaolinite clay are found to be 68.37, 13.35, 18.11, and 0.17%, respectively. Even though it has a high aggregation factor, the average hydrodynamic radius of kaolinite is found to be 250 nm. The ζ-potential value (−28.9 mV) of kaolinite clay indicates its moderate stability in water.

The surface morphology of the starch−glycerin film (Figure 1) gives a relatively smooth and continuous layer-by-layer morphology. In the starch−glycerin−montmorillonite nanocomposite film, nanoclay particles are homogeneously dispersed in the film. Better dispersion of clay indicates that exfoliation of clay may be obtained in the nanocomposite film. The plasticizer prevents the clay particles from aggregation owing to its hydrogen-bonding interaction with starch and montmorillonite. The elemental composition of the starch−glycerin−montmorillonite nanocomposite film is carbon, oxygen, sodium, aluminum, silicon, potassium, and calcium with atomic percentage of 78.76, 19.13, 0.25, 0.57, 1.53, 0.26, and 0.21%, respectively, which suggests successful incorporation of montmorillonite in the film. The starch−glycerin−hectorite nanocomposite film exhibits a rough, coral-like, and porous morphology. The clay exists mostly as either single platelets (exfoliation) or stacks of several platelets (intercalation). The elemental percentages of carbon, oxygen, sodium, magnesium, and silicon atoms are 80.29, 19.64, 0.01, 0.03, and 0.02%, respectively, which also confirm homogeneous incorporation of hectorite clay in the starch−glycerin−hectorite nanocomposite film. The layer-by-layer flake-type morphology is distinct for the starch−glycerin−kaolinite nanocomposite film. It contains carbon 80.59%, oxygen 19.19%, aluminum 0.19%, and silicon 0.09% by elemental mass, which also suggests the successful utilization of kaolinite clay to form the starch−glycerin−kaolinite nanocomposite film.

Native potato starch exhibits several characteristic absorption bands; the bands at 2935 and 3450 cm^{-1} correspond to hydroxyl group stretching, at 2924 and 1465 cm^{-1} to CH_2 stretching, at 1150 cm^{-1} to C−O bond stretching, at 1080 and 1040 cm^{-1} to C−O bond stretching of C−O−C groups in the anhydroglucose unit, and so on (Figure 2). In addition to the characteristic absorption bands of starch, additional absorption bands at different regions appeared for starch−plasticizer films as water, glycerin, ethylene glycol, sorbitol, and formamide have different hydrogen bond-forming abilities with the anhydroglucose ring of starch. The lower band intensity denotes the stronger interaction between starch and the plasticizer. For example, the characteristic bands of potato starch at 3450 and 1170 cm^{-1} shift toward downward frequency upon addition of glycerin, ethylene glycol, sorbitol, and formamide; the characteristic stretching bands for primary amides ($-NH_2$) at 3350 and 3180 cm^{-1} of formamide diminish in the starch−formamide film (Figure S2). The Fourier transform infrared (FTIR) spectrum of montmorillonite clay shows the characteristic absorption bands at 1100 cm^{-1} (Si−O), 522 cm^{-1} (Al−O), 463 cm^{-1} (Mg−O), 3630 cm^{-1}, and 3400 cm^{-1} (OH groups), etc. (Figure 2). The absorption bands corresponding to montmorillonite become sharp and their intensity increases with increasing loading of clay content in the starch−glycerin−montmorillonite nano-

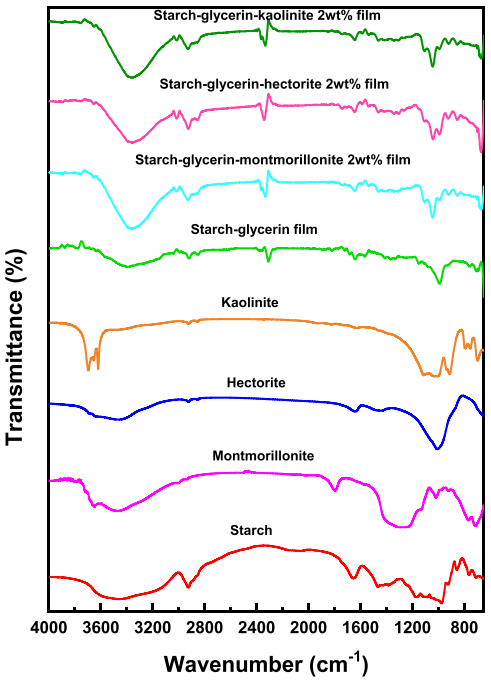

Figure 2. FTIR spectra of starch, montmorillonite, hectorite, kaolinite, starch−glycerin film, starch−glycerin−montmorillonite 2 wt % nanocomposite film, starch−glycerin−hectorite 2 wt % nanocomposite film, and starch−glycerin−kaolinite 2 wt % nanocomposite film.

https://dx.doi.org/10.1021/acsomega.0c02012
ACS Omega 2020, 5, 17543−17552

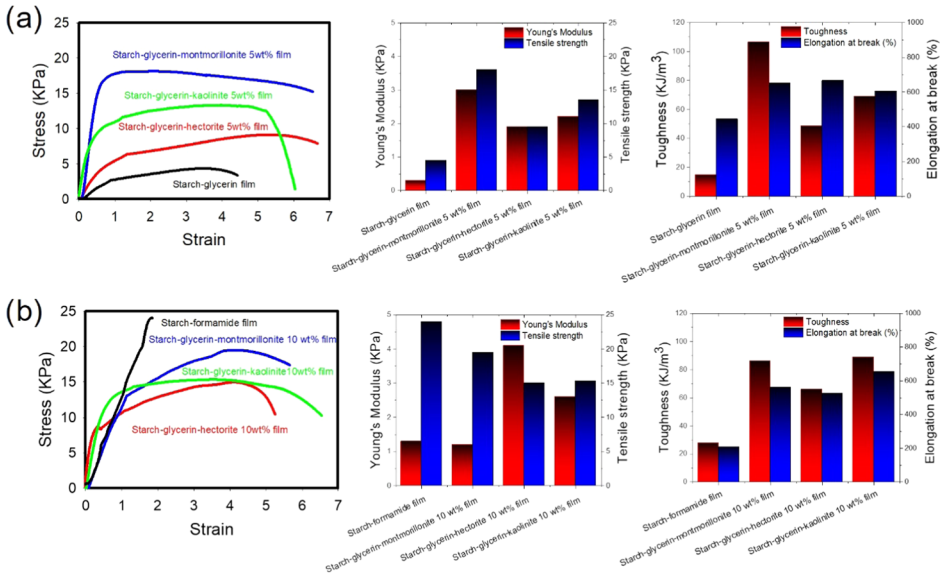

Figure 3. Stress−strain curves under uniaxial tension and the bar diagrams of Young's modulus, tensile strength, toughness, and elongation at break (%) for (a) starch−glycerin film, starch−glycerin−hectorite 5 wt % film, starch−glycerin−kaolinite 5 wt % film, and starch−glycerin−montmorillonite 5 wt % film and (b) starch−formamide film, starch−glycerin−hectorite 10 wt % film, starch−glycerin−kaolinite 10 wt % film, and starch−glycerin−montmorillonite 10 wt % film.

composite film (Figures S2−S8). The stretching frequencies of hydroxyl groups in hectorite clay give weak sharp bands at 3666 cm^{-1} and a broad band at 3620 cm^{-1}. The possible presence of Li and Mg carbonates in non-silicate phases of hectorite was confirmed from a band at approximately 1430 cm^{-1}. The Si−O band observed at 1000 cm^{-1} and the Mg−O band observed at around 460 cm^{-1} for hectorite nanoclay become clear with increasing hectorite content in the starch−glycerin−hectorite nanocomposite films. A typical FTIR spectrum of kaolinite gives four bands at 3697, 3669, 3645, and 3620 cm^{-1}, respectively; the band observed at 3620 cm^{-1} is due to the inner hydroxyl groups and the other bands are observed due to vibrations of external hydroxyl groups. The absorption bands observed at 1620−2642 cm^{-1} could be assigned to the −OH vibrational mode and the bands between 3450 and 3670 cm^{-1} are attributed to the −OH stretching mode. In the 1000 and 500 cm^{-1} region, Si−O and Al−OH bands are prominent. The absorption band of Al−OH is observed at 910 cm^{-1} and the Al−OH bending vibration bands are observed at 914 and 936 cm^{-1}. All of the above-mentioned characteristic bands of kaolinite are also observed in starch−clay−kaolinite nanocomposite films (Figure 2).

The plasticizer interacts with the starch polymer and lowers the intra- and intermolecular hydrogen bonding to increase the polymer mobility. Plasticizers are small in molecular size and hydrophilic, suppress retrogradation, and improve mechanical properties of thermoplastic starch. Glycerin produces a less stiff and highly ductile film compared with other plasticizers such as ethylene glycol, formamide, and sorbitol. This suggests that the starch molecules exist as highly flexible and coiled form while using glycerin, but their tensile strength, toughness, and Young's modulus are not well improved (Figure S9 and Table S9). We, therefore, focused our attention on starch−glycerin-based films with incorporation of three different types of nanoclays to improve these properties (Figure 3). The mechanical properties of the resulting nanocomposite films are dependent on the state of the nanoclay and starch polymers in the network, that is, whether the starch polymer is in the flocculated, intercalated, or exfoliated state in the network. The mechanical strength of the starch−glycerin−montmorillonite nanocomposite film decreases initially with addition of low percentage of clay and increases at optimum percentage of montmorillonite clay (Figures S10−S12 and Tables S10−S14). Owing to isomorphic substitution between metals, montmorillonite with negative charges can adsorb hydrated cations to enter the interlayer region, which then leads to an increase in the distance between adjacent layers. Accordingly, the whole surface layers including the internal surface and external surface can be hydrated, and the exchange reaction of cations can occur there, leading to the exfoliation and dispersion of the crystal along with starch polymers. The mechanical strength of starch−glycerin−hectorite nanocomposite films drastically increases after addition of hectorite clay compared with the starch−glycerin film. But their Young's modulus, tensile strength, and toughness are relatively low compared to starch−glycerin−montmorillonite films. The starch−glycerin−kaolinite nanocomposite film has intermediate Young's modulus and tensile strength compared with the other nanoclay-based films, but its toughness is the highest irrespective of the kaolinite content. Elongation at break of starch−glycerin−montmorillonite films increases with increasing montmorillonite content. The elongation at break values for the starch−glycerin film, starch−glycerin−montmorillonite 2 wt % film, starch−glycerin−montmorillonite 5 wt % film, and starch−glycerin−montmorillonite 10 wt % film are 445, 725, 650, and 562%, respectively. The elongation at break for the starch−glycerin−hectorite 2 wt % film is 400%, which increases to 666% for the starch−glycerin−hectorite 5 wt % film. If the hectorite content is further increased, elongation at break reduces to 526%, whereas the elongation at break for the starch−glycerin−kaolinite film gradually increases with increasing kaolinite content. The elongation at break values for the starch−glycerin−kaolinite 2 wt % film, starch−glycerin−kaolinite 5 wt % film, and starch−glycerin−kaolinite 10 wt % film are found to be 587, 606, and 655%, respectively. It can be concluded that the elongation at break values of all

https://dx.doi.org/10.1021/acsomega.0c02012
ACS Omega 2020, 5, 17543−17552

nanocomposite films are almost similarly high; i.e., irrespective of the nature of incorporated clays, all nanocomposite films are soft, flexible, ductile, and tough. Addition of nanoclays helps to improve the elongation at break of the films, as good dispersion of clay helps the starch polymer to anchor onto the exfoliated clay plates efficiently.

The XRD pattern of potato starch shows a characteristic crystalline peak at about 17.05° and amorphous peaks at 19.48, 22.14, and 24°. The amorphous peaks are broad and featureless, which indicates the semicrystalline nature of potato starch, and the XRD pattern of the potato starch matches well with the pattern of maize starch. The average crystallite size of montmorillonite, hectorite, and kaolinite was calculated as 26.1, 6.5, and 25.9 nm, respectively, which are much smaller compared with SEM and DLS values (Figures 4–6). The XRD

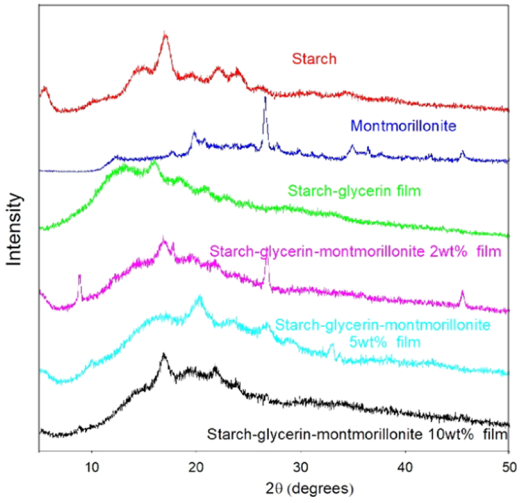

Figure 4. XRD patterns of starch–glycerin–montmorillonite nanocomposite films with varying montmorillonite amount.

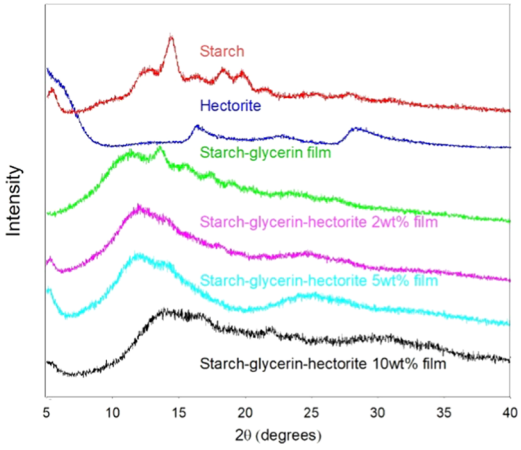

Figure 5. XRD patterns of starch–glycerin–hectorite nanocomposite films with varying hectorite amount.

patterns of montmorillonite, hectorite, and kaolinite also match well with those of their standard minerals. Upon incorporation of montmorillonite clay into the starch–glycerin film, the intensity of the crystalline peak of montmorillonite clay decreases with increasing clay percentage and the peak completely disappears in the starch–clay–montmorillonite 10 wt % nanocomposite film (Figure 4). But the crystalline

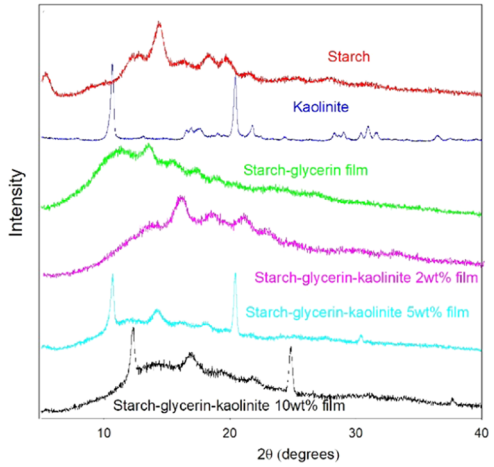

Figure 6. XRD patterns of starch–glycerin–kaolinite nanocomposite films with varying kaolinite amount.

peaks of montmorillonite are prominent in the starch–glycerin–montmorillonite 2 wt % nanocomposite film, which suggests that the use of 2 wt % montmorillonite is not suitable to obtain good biodegradable starch–glycerin–montmorillonite nanocomposite films. The XRD pattern of hectorite shows characteristic broad peaks at 19.48 and 34.94°, which suggest the semicrystalline and amorphous nature of hectorite nanoclay. Irrespective of the hectorite content (even using 2 wt %), starch–glycerin–hectorite nanocomposite films give highly broad and amorphous peaks, suggesting superior biocleavability (Figure 5). On the other hand, the XRD pattern of kaolinite exhibits characteristic crystalline peaks at 12.52 and 24.8° and several amorphous peaks (Figure 6). The crystalline peaks of kaolinite are not observed in the starch–glycerin–kaolinite 2 wt % nanocomposite film, but crystalline peaks are clearly visible with increasing kaolinite content. At a high kaolinite content, phase separation of kaolinite may have occurred due to the irregular distribution of clay particles inside nanocomposite film networks.

Depending on the relative distribution/dispersion of the stacks of clay platelets, three types of starch–clay nanocomposites are formed: an intercalated nanocomposite, where clay particles get into the polymer, resulting in a well-ordered multilayer morphology; a flocculated nanocomposite, where intercalated stacked clay particles are flocculated; and an exfoliated nanocomposite, where the clay particles are completely homogeneously dispersed in the polymer matrix. Because of the hydrophilic nature of starch, it has good miscibility in water with montmorillonite, hectorite, and kaolinite clays and they can easily intercalate/exfoliate into the interlayers.

The thermal degradation of potato starch and its nanocomposite films occurred in three steps. The first step (50–200 °C) is associated with the loss of water and plasticizer molecules, whereas the second step (200–350 °C) corresponds to the degradation of starch molecules, and the third step (400–900 °C) is assigned to the degradation of the clay (Figure 7). The decomposition temperature of the starch–glycerin film is 296 °C with an ash residue of 19%, but the starch–glycerin–montmorillonite nanocomposite film decomposes at 306 °C with an ash residue of 14%. All of the montmorillonite nanocomposite films exhibit an increase in the onset and midpoint temperature of degradation relative to

https://dx.doi.org/10.1021/acsomega.0c02012
ACS Omega 2020, 5, 17543–17552

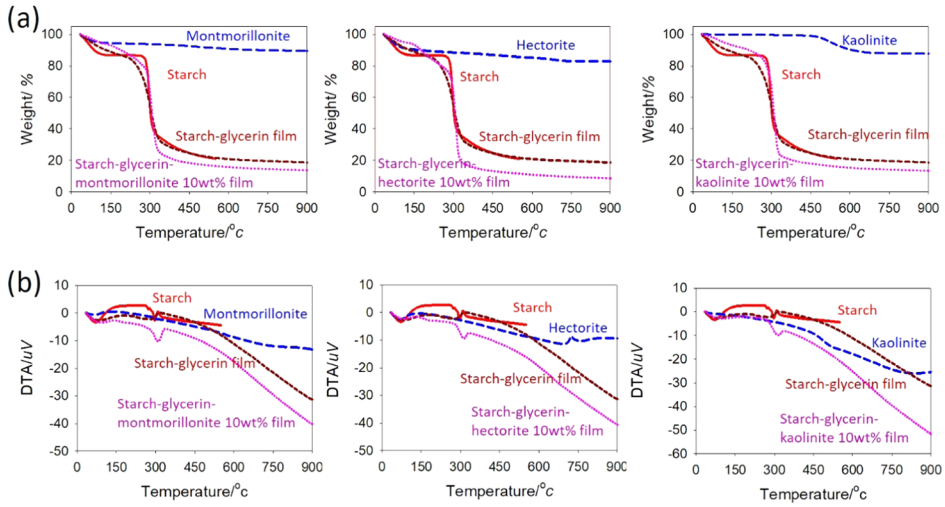

Figure 7. (a) Thermogravimetric (TG) curves of starch and montmorillonite, hectorite, and kaolinite based nanocomposite films and (b) DTA curves of starch and montmorillonite, hectorite, and kaolinite based nanocomposite films.

starch−glycerin films, which increases with increasing montmorillonite content, indicating enhanced thermal resistance. In the starch−glycerin−montmorillonite nanocomposite film, the content of starch and glycerin is slightly higher than in the starch−glycerin film, which gives a relatively lower ash residue. Hectorite decomposes at 720 °C with an ash residue of 83% at 900 °C. The starch−glycerin−hectorite nanocomposite film (decomposes at 316 °C with an ash residue of 9%) also exhibits better thermal stability compared to the starch−glycerin film. The kaolinite decomposes at two plateau regions; the first decomposition starts at 470 °C, and the second decomposition starts at 790 °C. Only 20% weight loss is observed at 900 °C. The starch−glycerin−kaolinite nanocomposite film decomposes at 311 °C with an ash residue of 13%. The interactions among starch, glycerin, and kaolinite in starch−glycerin−kaolinite nanocomposite films are much stronger than in starch−glycerin films, resulting in better thermal stability of the films.

The water absorption of the starch-based film decreases with the plasticizer addition and further decreases with the addition of clay. With addition of different types of plasticizer such as glycerin, ethylene glycol, sorbitol, and formamide into starch-based films, water absorption is almost the same except for sorbitol, which has the lowest water absorption capacity (Figures S13−S16). The water absorption of all nanocomposite films is significantly reduced compared to the starch film, and no appreciable change is observed for starch−glycerin−hectorite, starch−glycerin−montmorillonite, and starch−glycerin−kaolinite nanocomposite films (Figure 8). Amylopectin of starch is more sensitive to glycerin plasticization than amylose. As amylopectin percentage in potato starch is about 70% in most cases, water absorption significantly decreases to 60%. In addition, the presence of nanoclay directly affects the crystallinity of starch to show low water absorption. The starch film takes up water readily up to 125%, but with addition of glycerin, it reduces to 90% and decreases further with increasing montmorillonite/hectorite content. Owing to the low cation exchange capacity of kaolinite, water molecules cannot enter the interlayer space to behave as a nonswelling type of clay. The presence of kaolinite thus significantly reduces the water uptake percentage of starch−glycerin−kaolinite nanocomposite films. Generally,

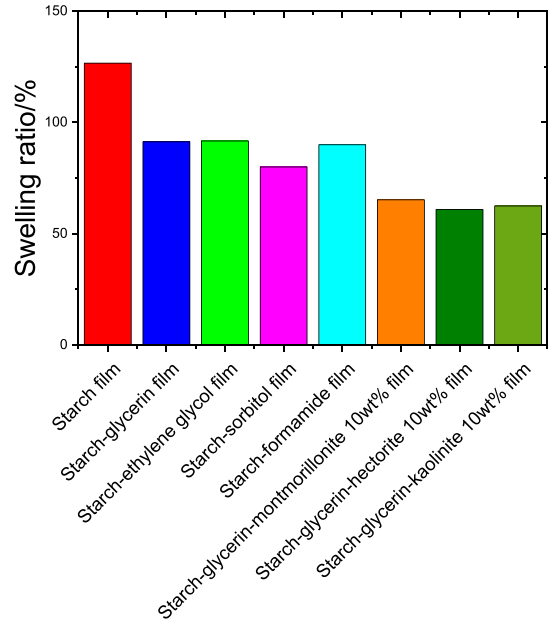

Figure 8. Percentage of swelling ratio in water with time for starch-based films by varying the type of plasticizer and nanoclay.

water absorption through a hydrophilic film depends on both diffusivity and solubility of water molecules in the film matrix. When the nanocomposite structure is formed, the impermeable clay layers mandate a tortuous pathway for water molecules to traverse the film matrix, thereby increasing the effective path length for diffusion. The decreased diffusivity due to the homogeneous mixing of clay with starch in starch−plasticizer−clay nanocomposite films reduced the water absorption capacity. In summary, the native starch film showed the highest water absorption capacity. It decreases with the addition of different plasticizers and further decreases with addition of different types of clays. The water uptake percentage followed the order starch film > starch−plasticizer film > starch−glycerin−montmorillonite nanocomposite film > starch−glycerin−kaolinite nanocomposite film > starch−glycerin−hectorite nanocomposite film.

https://dx.doi.org/10.1021/acsomega.0c02012
ACS Omega 2020, 5, 17543−17552

CONCLUSIONS

In this work, a natural biodegradable polymer starch has successfully been extracted from potato. Different types of plasticizers and various nanoclays were used with extracted potato starch to fabricate starch-based nanocomposite films by a facile and simple solution casting method. Glycerin was the most effective plasticizer for starch−plasticizer composite films, which increased the tensile strength appreciably compared to sorbitol, ethylene glycol, formamide, and other plasticizers. Incorporated clay particles were homogeneously dispersed into starch−plasticizer−clay nanocomposite films to form an intercalated/exfoliated network using optimum percentage of clay. All types of clays such as hectorite, montmorillonite, and kaolinite can significantly improve the mechanical properties, thermal stability, and water resistivity of starch−clay nanocomposite films. Suitable physical interactions and formation of the intercalation or exfoliation network are responsible for these interesting phenomena. The crystalline peaks of potato starch and clays are found to be amorphous peaks in the nanocomposite films, which indicates the superior biodegradable properties of potato starch-based nanocomposite films. Starch−plasticizer−clay nanocomposite films are a valuable addition to the existing film materials and eventually can substitute petroleum-based composite films in numerous applications due to their inherent advantages such as biodegradability, ecofriendliness, low cost, and easy availability. The synthesized starch−clay nanocomposite films are environmentally friendly, which could significantly reduce the negative environmental impact in terms of energy consumption and the greenhouse effect compared with the traditional nondegradable polymeric materials. They may potentially be used as alternatives to synthetic plastic materials, plastic bags, drug delivery systems, smart sensors, fuel cells, and so on.

EXPERIMENTAL SECTION

Materials. Montmorillonite (Sigma-Aldrich, Japan), hectorite (Wako, Japan), kaolinite (Fluka, Japan), glycerin (Merck, Germany), sorbitol (Merck, Germany), formamide (Merck, Germany), and ethylene glycol (S.D. Fine Chemicals Ltd., India) were purchased and used as received. Deionized water, unless otherwise noted, was used throughout the work.

Extraction of Starch from Potato. Briefly, 500 g of potato was weighed and cut into very tiny size using a commercially available fine vegetable slicer. Then, 1 L of distilled water was mixed with the paste and stirred properly using a glass rod until water color changed to purple. Then, the liquid portion of the potato juice was separated with a fine mesh, poured into a Petri dish, and kept for 3−4 h at room temperature. Starch particles settled down in the Petri dish. The settled starch particles were washed several times with distilled water and dried at 105 °C in an oven to remove any residual water. The percent yield of the extracted potato starch was 10 wt %. A schematic diagram of extraction of starch from potato is given in Scheme 1.

Preparation of Starch−Plasticizer Composite Films. The extracted starch powder (800 mg) was added into 13 mL of distilled water in a vial. Then, 30 wt % plasticizer (water/glycerin/ethylene glycol/sorbitol/formamide) was mixed in another vial and was added slowly into the starch suspension while stirring. The mixture was heated in an oil bath at 70 °C allowing the gradual evaporation of the solvent. Then the suspension was poured into a polyethylene sheet and vacuum-dried at 40 °C. By maintaining the amount of suspension, the thickness of the starch−plasticizer film can be precisely controlled (Scheme S1).

Scheme 1. Schematic Representation of Preparation of Starch−Plasticizer−Clay Nanocomposite Films

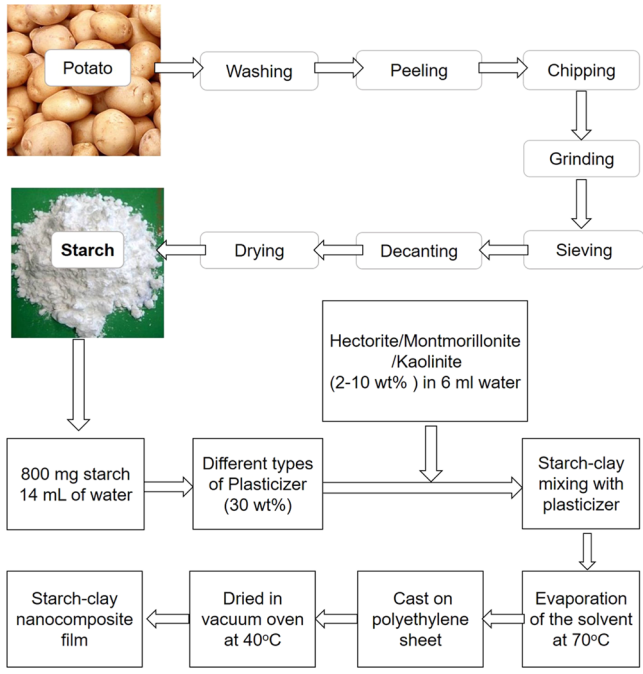

Preparation of Starch−Plasticizer−Clay Nanocomposite Films. Starch (800 mg) was added into 14 mL of water upon heating. Then, 30 wt % of different types of plasticizers (water/glycerin/ethylene glycol/sorbitol/formamide) was used to improve the compatibility between the hydrophilic starch granules and nanoclay particles. In another container, 2−10 wt % montmorillonite/hectorite/kaolinite nanoclay was dispersed in water using an ultrasonic bath for 30 m and was added slowly into the starch suspension with continuous stirring. The mixture of starch, plasticizer, and nanoclay was stirred constantly for several hours at 70 °C allowing the evaporation of the solvent. The suspension was then poured into a polyethylene sheet and kept under vacuum at 40 °C to obtain starch−plasticizer−clay nanocomposite films (Figure S1). Tables S1−S8 represent the recipes of different types of fabricated potato starch-based nanocomposite films.

Dynamic Light Scattering (DLS). Dynamic light scattering measurements were performed using a Zetasizer Nano ZS from Malvern Instruments to measure the hydrodynamic radius of samples. About 1 wt % aqueous solutions or suspensions of potato starch and montmorillonite, hectorite, and kaolinites clay were prepared and stirred vigorously. The dispersed samples were then sonicated for 30 m and allowed to settle down before measurements. A laser beam of 532 nm wavelength was illuminated on the samples at room temperature for analysis. The intensity fluctuation of the scattered light was analyzed to determine the hydrodynamic radius. The ζ-potential of the samples was measured using a universal dip cell in conjunction with a disposable polystyrene cell.

Scanning Electron Microscopy (SEM). The surface morphology of the synthesized nanocomposite films was studied by field emission scanning electron microscopy (FE-SEM) using a JEOL JSM-7600F (LabWrench, Japan). The

https://dx.doi.org/10.1021/acsomega.0c02012
ACS Omega 2020, 5, 17543−17552

dried and powdered samples were sputtered with platinum to obtain a very thin platinum layer to ensure sufficient conductivity of the sample surface. The microscope was operated at an accelerating voltage of 5.0 kV. The elemental compositions of the samples were determined by an energy-dispersive X-ray spectrometer (EDS) coupled with the FE-SEM.

Fourier Transform Infrared (FTIR) Spectroscopy. The infrared spectra were recorded by a Fourier transform infrared spectrophotometer (Frontier FT-NIR/MIR, PerkinElmer) in the region of 4000−400 cm^{-1}. The samples were oven-dried at 60 °C and ground in a mortar with a pestle to get the powder. The sample disk was prepared by maintaining the "sample-to-KBr" ratio as 1:100.

Attenuated Total Reflectance (ATR). The FTIR spectrometer equipped with a horizontal attenuated total reflectance (HATR) cell was used for analyzing strongly absorbing or thick samples. The sample films were cut into a rectangular shape with dimensions 70 mm × 20 mm × 0.1 mm and were then directly placed on a Zn−Se plate before measurements. Each sample was scanned 30 times and the scanning resolution was 4 cm^{-1}.

Mechanical Tests. The film samples with dimensions of 70 mm × 20 mm × 0.1 mm were used for uniaxial tensile measurements. The tensile measurements were conducted by a universal testing machine (UTM Instron 3369) at ambient temperature. The load cell used for the tensile test was an Instron static load cell with a 50 kN capacity. The crosshead speed was 2 mm/min. Each specimen was tested at least three times to check the reproducibility. The tensile stress (σ) of the films was obtained from the recorded force and area data, whereas the strain was calculated from the ratio of the change in length (Δl) and the initial length (l) of the sample. The Young's modulus, toughness, tensile strength, and elongation at break of the sample films were calculated from the stress−strain curve.

X-ray Diffraction (XRD). An X-ray diffractometer (D8 Advance, Bruker Optik, Ettlingen, Germany) with Cu Kα radiation (λ = 1.5406 Å) and working at 40 kV/40 mA in the range of 10−80° with 0.02° scan step and a 2°/min scanning rate was used. The film samples for XRD were prepared by the solution casting method and cut into a rectangular shape with dimensions 30 mm × 10 mm × 0.1 mm. The XRD diffraction data were analyzed using the diffract plus EVA 16.0 software, and the average crystallite size of starch and nanoclays was determined using the Scherrer equation

$$t = k\lambda/\beta \cos\theta$$

where t is the crystallite size, β is the full width at half-maximum of the peak, and k is a constant.

Thermogravimetry and Differential Thermal Analysis (TG−DTA). TG/DTA data were measured by a DT/TGA 7200 (HITACHI, Japan). For each measurement, about 5 mg of dried and powdered sample was taken in a platinum sample pan and analyzed from room temperature to 900 °C at a heating rate of 10 °C/min under a nitrogen atmosphere.

Nitrogen gas was purged at a flow rate of 20 mL/min.

Water Absorption Test. A circular piece of 0.1 mm thickness and 12 mm diameter of the film sample was dried in an oven at 105 °C for about 2 h and was immersed in a large amount of deionized water. The film was swelled at room temperature for 1 day and allowed to reach the swelling equilibrium state. The equilibrium swelling ratio or water content is calculated using the following equation

$$\text{swelling ratio } (\%) = (W_{wet} - W_{dry})/W_{dry} \times 100$$

where W_{wet} is the weight of the swollen film after equilibrium and W_{dry} is the weight of the dry film. Excess water on the surface of the film samples was wiped off by tissue before taking the weight of samples. Three specimens from each category were tested to check the reproducibility.

■ ASSOCIATED CONTENT

Supporting Information

The Supporting Information is available free of charge at https://pubs.acs.org/doi/10.1021/acsomega.0c02012.

Recipe for preparation of potato starch-based films (Tables S1−S8); tensile properties of potato starch-based films (Tables S9−S14); schematic representation of preparation of potato starch−plasticizer films (Figure S1); photographs of potato starch-based films (Figure S2); FTIR spectra of potato starch, nanoclay, and their films (Figures S2−S8); stress−strain curves under uniaxial tension for potato starch-based films (Figures S9−S12); percentage of swelling ratio in water with time for potato starch-based films (Figures S13−S16) (PDF)

■ AUTHOR INFORMATION

Corresponding Author

Abu Bin Imran − *Department of Chemistry, Faculty of Engineering, Bangladesh University of Engineering and Technology, Dhaka 1000, Bangladesh;* orcid.org/0000-0001-8920-8921; Email: abimran@chem.buet.ac.bd

Authors

Hasanul Banna Muhammad Zukaul Islam − *Department of Chemistry, Faculty of Engineering, Bangladesh University of Engineering and Technology, Dhaka 1000, Bangladesh*

Md. Abu Bin Hasan Susan − *Department of Chemistry, Faculty of Science, University of Dhaka, Dhaka 1000, Bangladesh;* orcid.org/0000-0003-0752-1979

Complete contact information is available at: https://pubs.acs.org/10.1021/acsomega.0c02012

Notes

The authors declare no competing financial interest.

■ ACKNOWLEDGMENTS

A.B.I. gratefully acknowledges the support of the Grant of Advanced Research in Education (GARE) (PS2016239) from the Ministry of Education, People's Republic of Bangladesh. The author is also grateful to the Committee for Advanced Studies and Research (CASR) in BUET and The World Academy of Sciences (TWAS), Italy, a program of UNESCO (16-157 RG/CHE/AS_I − FR3240293340) for funding.

■ REFERENCES

(1) Hizukuri, S.; Takeda, Y.; Maruta, N.; Juliano, B. Molecular Structures Of Rice Starch. *Carbohydr. Res.* **1989**, *189*, 227−235.

(2) Ao, Z.; Jane, J. Characterization and modeling of the A- and B-granule starches of wheat, triticale and barley. *Carbohydr. Polym.* **2007**, *67*, 46−55.

(3) Aníbal, M. S.; Maria, A. B.; Margarita, A. Water barrier properties of starch-clay nanocomposite films. *Braz. J. Food Technol.* **2012**, *15*, 208−218.
(4) Zdanowicz, M.; Johansson, C. Impact Of Additives On Mechanical And Barrier Properties Of Starch-Based Films Plasticized With Deep Eutectic Solvents. *Starch - Stärke* **2017**, *69*, No. 1700030.
(5) Yang, J.; Yu, J.; Ma, X. Preparation of a novel thermoplastic starch (TPS) material using ethylenebisformamide as the plasticizer. *Starch - Stärke* **2006**, *58*, 330−337.
(6) Ma, X.; Yu, J. Formamide as the plasticizer for thermoplastic starch. *J. Appl. Polym. Sci.* **2004**, *93*, 1769−1773.
(7) Wang, L.; Shogren, R. L.; Carriere, C. Preparation and properties of thermoplastic starch-polyester laminate sheets by coextrusion. *Polym. Eng. Sci.* **2000**, *40*, 499−506.
(8) Kirby, A. R.; Clark, S. A.; Parker, R.; Smith, A. C. The deformation and failure behaviour of wheat starch plasticized with water and polyols. *J. Mater. Sci.* **1993**, *28*, 5937−5942.
(9) Otey, F. H.; Mark, A. M.; Mehltretter, C. L.; Russell, C. R. Starch based film for degradable agricultural mulch. *Ind. Eng. Chem. Prod. Res. Dev.* **1974**, *13*, 90−92.
(10) Lawton, J. W.; Fanta, G. F. Glycerol-plasticized films prepared form starch-poly(vinyl alcohol) mixtures: effect of poly(ethylene-co-acrylic acid). *Carbohydr. Polym.* **1994**, *23*, 275−280.
(11) Otey, F. H.; Westhoff, R. P.; Doane, W. M. Starch based blown films. *Ind. Eng. Chem. Prod. Res. Dev.* **1980**, *19*, 592−595.
(12) Xie, W.; Pan, W.; Chuang, K. Thermal characterization of PMR polyimides. *Thermochim. Acta* **2001**, *367*−*368*, 143−153.
(13) Coleman, J.; Khan, U.; GunKo, Y. Mechanical reinforcement of polymers using carbon nanotubes. *Adv. Mater.* **2006**, *18*, 689−706.
(14) Patil, A.; Vaia, R.; Dai, L. Surface modification of aligned carbon nanotube arrays for electron emitting applications. *Synth. Met.* **2005**, *154*, 229−232.
(15) Schmidt, D.; Shah, D.; Giannelis, E. New advances in polymer/layere silicate nanocomposites. *Curr. Opin. Solid State Mater. Sci.* **2002**, *6*, 205−212.
(16) Okada, A.; Usuki, A. Twenty years of polymer-clay nanocomposites. *Macromol. Mater. Eng.* **2006**, *291*, 1449−1476.
(17) Powell, C.; Beall, G. Physical properties of polymer/clay nanocomposites. *Phys. Prop. Polym. Handb.* **2006**, *136*, 561−575.
(18) Podsiadlo, P.; Choi, S.; Shim, B.; Lee, J.; Cuddihy, M.; Kotov, N.; et al. Molecularly engineered nanocomposites: Layer-by-layer assembly of cellulose nanocrystals. *Biomacromolecules* **2005**, *6*, 2914−2918.
(19) Hussain, F.; Hojjati, M.; Okamoto, M.; Gorga, R. Review article: polymer-matrix nanocomposites, processing, manufacturing, and application: an overview. *J. Compos. Mater.* **2006**, *40*, 1511−1575.
(20) Cho, D.; Lee, S.; Yang, G.; Fukushima, H.; Drzal, L. Dynamic mechanical and thermal properties of phenylethynyl-terminated polyimide composites reinforced with expanded graphite nanoplatelets. *Macromol. Mater. Eng.* **2005**, *290*, 179−187.
(21) Sevostianov, I.; Kachanov, M. Effect of interphase layers on the overall elastic and conductive properties of matrix composites Applications to nanosize inclusion. *Int. J. Solids Struct.* **2007**, *44*, 1304−1315.
(22) Nair, L. S.; Laurencin, C. T. Biodegradable polymers as biomaterials. *Prog. Polym. Sci.* **2007**, *32*, 762−798.
(23) Sinha Ray, S.; Okamoto, M. Polymer/layered silicate nanocomposites: A review from preparation to processing. *Prog. Polym. Sci.* **2003**, *28*, 1539−1641.
(24) Lu, D. R.; Xiao, C. M.; Xu, S. J. Starch-based completely biodegradable polymer materials. *eXPRESS Polym. Lett.* **2009**, *3*, 366−375.
(25) Kojima, Y.; Usuki, A.; Kawasumi, M.; Okada, A.; Kurauchi, T.; Kamigaito, O. Synthesis of nylon 6-clay hybrid by montmorillonite intercalated with 2-caprolactam. *J. Polym. Sci., Part A: Polym. Chem.* **1993**, *31*, 983−986.
(26) Okada, A.; Usuki, A. The chemistry of polymer-clay hybrids. *Mater. Sci. Eng., C* **1995**, *3*, 109−115.
(27) Lan, T.; Pinnavaia, T. Clay-reinforced epoxy nanocomposites. *Chem. Mater.* **1994**, *6*, 2216−2219.
(28) Yano, K.; Usuki, A.; Okada, A. Synthesis and properties of polyimide clay hybrid films. *J. Polym. Sci., Part A: Polym. Chem.* **2000**, *35*, 2289−2294.
(29) Fukushima, Y.; Inagaki, S. Synthesis of an intercalated compound of montmorillonite and 6-polyamide. *J. Inclusion Phenom.* **1987**, *5*, 473−482.
(30) Vaia, R.; Jandt, K.; Kramer, E.; Giannelis, E. Kinetics of polymer melt intercalation. *Macromolecules* **1995**, *28*, 8080−8085.
(31) Chen, T.; Tien, Y.; Wei, K. Synthesis and characterization of novel segmented polyurethane/clay nanocomposite. *Polymer* **2000**, *41*, 1345−1353.
(32) Hasegawa, N.; Okamoto, H.; Kato, M.; Usuki, A. Preparation and mechanical properties of polypropylene-clay hybrids based on modified polypropylene and organophilic clay. *Appl. Polym. Sci.* **2000**, *78*, 1918−1922.
(33) Reichert, P.; Hoffmann, B.; Bock, T.; Thomann, R.; Mulhaupt, R.; Friedrich, C. Morphological stability of poly (propylene) nanocomposites. *Macromol. Rapid Commun.* **2001**, *22*, 519−523.
(34) Nam, P.; Maiti, P.; Okamoto, M.; Kotaka, T.; Hasegawa, N.; Usuki, A. A hierarchical structure and properties of intercalated polypropylene/clay nanocomposites. *Polymer* **2001**, *42*, 9633−9640.
(35) Liu, X.; Wu, Q. PP/clay nanocomposites prepared by grafting-melt intercalation. *Polymer* **2001**, *42*, 10013−10019.
(36) Zhang, Q.; Wang, Y.; Fu, Q. Shear-induced change of exfoliation and orientation in polypropylene/montmorillonite nanocomposites. *J. Polym. Sci., Part B: Polym. Phys.* **2003**, *41*, 1−10.
(37) Rong, J.; Jing, Z.; Li, H.; Sheng, M. A polyethylene nanocomposite prepared via insitu polymerization. *Macromol. Rapid Commun.* **2001**, *22*, 329−334.
(38) Wang, K.; Choi, M.; Koo, C.; Choi, Y.; Chung, I. Synthesis and characterization of maleated polyethylene/clay nanocomposites. *Polymer* **2001**, *42*, 9819−9826.
(39) Park, H. M.; Li, X.; Jin, C. Z.; Park, C. Y.; Cho, W. J.; Ha, C. S. Preparation and properties of biodegradable thermoplastic starch/clay hybrids. *Macromol. Mater. Eng.* **2002**, *287*, 553−558.
(40) Park, H. M.; Lee, W. K.; Park, C. Y.; Cho, W. J.; Ha, C. S. Environmentally friendly polymer hybrids: part I—mechanical, thermal, and barrier properties of thermoplastic starch/clay nanocomposites. *J. Mater. Sci.* **2003**, *38*, 909−915.
(41) Huang, M. F.; Yu, J. G.; Ma, X. F. Studies on the properties of montmorillonite-reinforced thermoplastic starch composites. *Polymer* **2004**, *45*, 7017−7023.
(42) Wilhelm, H. M.; Sierakowski, M. R.; Souza, G. P.; Wypych, F. Starch films reinforced with mineral clay. *Carbohydr. Polym.* **2003**, *52*, 101−110.
(43) McGlashan, S. A.; Halley, P. J. Preparation and characterization of biodegradable starch-based nanocomposite materials. *Polym. Int.* **2003**, *52*, 1767−1773.
(44) Kalambur, S. B.; Rizvi, S. S. H. Starch-based nanocomposites by reactive extrusion processing. *Polym. Int.* **2004**, *53*, 1413−1416.
(45) Tang, X.; Sajid, A.; Thomas, J. H. Barrier and Mechanical Properties of Starch-Clay Nanocomposite Films. *Cereal Chem. J.* **2008**, *85*, 433−439.
(46) Kiliaris, P.; Papaspyrides, C. D. Polymer/layered silicate (clay) nanocomposites: An overview of flame retardancy. *Prog. Polym. Sci.* **2010**, *35*, 902−958.
(47) Chen, B.; Julian, R. G. E. Thermoplastic starch−clay nanocomposites and their characteristics. *Carbohydr. Polym.* **2005**, *61*, 455−463.
(48) Hwan-Man, P.; Xiucuo, L.; Chang-Zhu, J.; Chan-Young, P.; Won-Jei, C.; Chang-Sik, H. Preparation and Properties of Biodegradable Thermoplastic Starch/Clay Hybrids. *Macromol. Mater. Eng.* **2002**, *287*, 553−558.
(49) Avella, M.; Jan, J. D. V.; Maria, E. E.; Sabine, F.; Paolo, V.; Maria, G. V. Biodegradable starch/clay nanocomposite films for food packaging applications. *Food Chem.* **2005**, *93*, 467−474.

https://dx.doi.org/10.1021/acsomega.0c02012
ACS Omega 2020, 5, 17543−17552

(50) Yu, L.; Katherine, D.; Lin, L. Polymer blends and composites from renewable resources. *Prog. Polym. Sci.* **2006**, *31*, 576−602.
(51) Wang, N.; Yu, J. G.; Chang, P. R.; Ma, X. Influence of formamide and water on the properties of thermoplastic starch/poly(lactic acid) blends. *Carbohydr. Polym.* **2008**, *71*, 109−118.
(52) van Jeroen, J. J. G.; Remko, C. B.; Dick, D. W.; Johannes, F. G. V. Influence of glycerol on the melting of potato starch. *Ind. Crops Prod.* **1996**, *5*, 1−9.

https://dx.doi.org/10.1021/acsomega.0c02012
ACS Omega 2020, 5, 17543−17552